

## Fault Localization in Contact Level by Using Conductive Atomic Force Microscopy

Jon C. Lee, J. H. Chuang

Taiwan Semiconductor Manufacturing Company, Ltd., Hsin-Chu, Taiwan

### Abstract

As integrated circuits (IC) have become more complicated with device features shrinking into the deep sub-micron range, so the challenge of defect isolation has become more difficult. Many failure analysis (FA) techniques using optical/electron beam and scanning probe microscopy (SPM) have been developed to improve the capability of defect isolation.

SPM provides topographic imaging coupled with a variety of material characterization information such as thermal, magnetic, electric, capacitance, resistance and current with nano-meter scale resolution. Conductive atomic force microscopy (C-AFM) has been widely used for electrical characterization of dielectric film and gate oxide integrity (GOI). In this work, C-AFM has been successfully employed to isolate defects in the contact level and to discriminate various contact types. The current mapping of C-AFM has the potential to identify micro-leaky contacts better than voltage contrast (VC) imaging in SEM. It also provides I/V information that is helpful to diagnose the failure mechanism by comparing I/V curves of different contact types.

C-AFM is able to localize faulty contacts with pico-amp current range and to characterize failure with nano-meter scale lateral resolution. C-AFM should become an important technique for IC fault localization. FA examples of this technique will be discussed in the article.

### Introduction

As device complexity increases and feature sizes reduce further, non-visible defects such as junction leakage, crystal defect and gate leakage will become an important root cause for IC failure. Therefore, failure analysis has become significantly more difficult, especially failure site localization. Successful failure analysis requires an effective method of defect isolation. Failure to identify the fault location will result in an inability to carry out a physical failure analysis (PFA). Many existing localization techniques such as EMMI (with or

without Mercury Cadmium Telluride detector), liquid crystal (LC), Light Induced Voltage Alteration (LIVA), Thermal Induced Voltage Alteration (TIVA), Seebeck Effect Imaging (SEI), Optical Beam Induced Resistance Change (OBIRCH), Optical Beam Induced Current (OBIC)... etc. have already been widely used. However, the emission hot spots detected by these techniques may be large and cover several elements (device, via or contact). This means that conventional techniques are not precise enough by themselves to pin point defects in today's devices. Combining these techniques with layout tracing and passive voltage contrast (PVC) can improve the accuracy of defect isolation and increase the FA success rate.

Passive voltage contrast technique has recently been applied to contact level inspection using electron beam or ion beam to precisely isolate abnormal contacts. This method is able to recognize abnormal contacts that suffer leakage or higher resistance. However, PVC is still not able to isolate defects in all cases. This is true even when steps are taken to improve the sensitivity of the passive voltage contrast technique [1]. Internal probing may offer a solution to identify faulty contacts by directly current measurement on individual contacts. Conventional micro-probing using etched tungsten needles or probes, mounted to manipulators on a probe station or in a SEM chamber are not accurate enough to probe small features. It is also easy to wear the probe tip. This probing technique will therefore not satisfy the demand of failure analysis and defect characterization for deep sub-micron technology.

Krieg et al. have reported AFM based nano-probing [2,3] in which the scanning tip of an AFM is used for probing as well as imaging. The probe tip is very sharp, thus making image resolution better than 50nm and two probe contact points could be less than 0.25um apart (hardware constraints with current AFM designs prohibit this). Andrew Erickson announced an Atomic Force Probing (AFP) system in 2002 [4]. Etched tungsten wire probes were used in this system and the radius of tip is nominally less than 90nm. Contact level I/V measurement of array

devices with AFP has been demonstrated at 0.25, 0.18, and 0.13 $\mu\text{m}$  technology nodes. For these two systems multiple probes can be used for signal measurement and they are all based on AFM practices to control the movement of the probe and the applied force.

C-AFM is a common tool for most semiconductor FA laboratories to study gate oxide integrity (GOI) and dielectric breakdown. Furthermore, the determination of local effective oxide thickness in the sub-angstrom range by C-AFM was introduced in 2000 [5]. The oxide thickness is obtained by fitting the local I/V curve to the well-known Fowler-Nordheim tunneling equation. In this article C-AFM has been used to precisely isolate defects for contact micro-leakage or higher contact resistance, and to characterize defects by local I/V measurements from contacts to substrate.

C-AFM has the ability to scan the sample with nano-meter scale lateral resolution and to measure the current in the pico-amp range. Topography and current data are obtained simultaneously. Analysis of the current map will yield faulty contacts in the form of a gray scale and can be identified quickly and easily. C-AFM may be utilized further as a nano-probe to provide local I/V measurements for specific features (contacts). The current map may not show obvious defects and so the ability to directly compare I/V curves of individual contacts is helpful in identifying anomalies.

## Experimental setup

A Digital Instruments Dimension 3100 AFM with a NanoScope IV controller and a C-AFM application module was used in this experiment. The C-AFM module can be operated in either imaging or spectroscopy (I/V) mode. In imaging mode, a conductive tip is scanned over the sample surface in contact mode with the deflection of cantilever kept constant and the local height of the sample measured. While scanning, DC bias can be applied between the sample (stage) and tip in the range of  $\pm 12\text{V}$ . A low noise linear current amplifier with a noise level of around 1pA RMS and a current measurement range from 1pA to 1uA simultaneously maps the tip-sample current as the topography is measured. A schematic of the experimental setup is shown in Figure 1 [6].

C-AFM can also measure local current-voltage (I/V) spectra for specific locations using spectroscopy mode. In order to obtain a local I/V curve the imaging scan is stopped and the tip is held at a fixed location while the sample bias is ramped. The tip-sample current is plotted versus the applied bias. A closed-loop scanner is required to accurately move the tip to a specific position (contacts) and to prevent drifting during the I/V measurement.

Samples lapped the contact level yield tungsten features that are extremely sharp and able to destroy a metal-coated probe

very quickly. For this reason, conductive boron doped diamond tips were used in this experiment. The conductivity of these probes is around 0.003 to 0.005  $\Omega\text{-cm}$ .

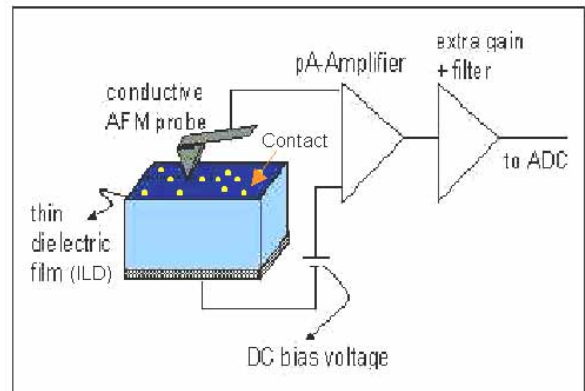


Figure 1: Schematic representation of Conductive AFM (C-AFM) setup.

## Case study

### Various contacts identification

The sample of study was a 6T SRAM manufactured using a standard CMOS process. Each bit is composed of six transistors and ten contacts (including two common bit-line contacts and one common  $V_{\text{dd}}$  contact). The sample was parallel lapped to the contact level. VC examination was then performed using a SEM. The VC image shows clear contrast for the different types of contact within the image, Figure 2.

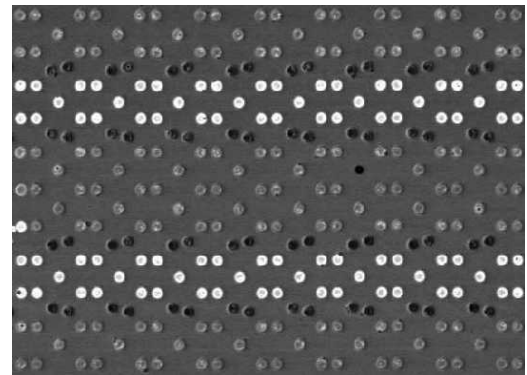


Figure 2: VC image shows different types of contact with clear contrast difference under  $V_{\text{acc}}$  at 1kV.

The gray levels of the figure 2 correspond to  $\text{P}^+$  contact; bright,  $\text{N}^+$  contact; dark gray and poly contact; black. The SEM acceleration voltage was 1kV. Under these conditions an accumulation of positive charge is produced at the contacts. For  $\text{P}^+$  contacts, the structure behaves like a forward-biased diode ( $\text{P}^+/\text{N}$ -well); the positive charge can drain off, so the

resulting contrast is bright. For  $N^+$  contacts, the structure behaves like a reverse-biased diode ( $N^+/P$ -well). Part of the positive charge drains away and the structure reaches reverse saturation, most positive charge still accumulates, and then dark contrast is observed. For poly contacts, only little positive charge (relative to the total build-up positive charges) leaks to substrate through gate oxide, most of the positive charge (more than that of the  $N^+$  case) accumulates, so the contrast is the black in the VC image [1].

Samples were then measured with C-AFM and the results compared to those obtained from VC. The tip-sample current was measured with an applied bias of  $-2V$  as the tip was scanned across the sample surface. The corresponding current map, Figure 3 also shows three distinct levels corresponding to the different contacts. The darker spots are  $P^+$  contacts, the intermediate spots are poly contact, and the lighter spots are  $N^+$  contact. Different color indicates a different current level with the darker indicating a higher current.  $P^+$  contacts show the characteristics of a forward-biased diode ( $P^+/N$ -well) and are dark in color. For  $N^+$  contacts, the system looks like a reverse-biased diode ( $N^+/P$ -well) and only reverse saturation current exists. Hence they are lighter in color. The gray scale is reversed as the sample bias is set to a positive voltage. For poly contacts, Fowler-Nordheim tunneling exists for gate oxide thickness  $d_{ox} > 2.5nm$  where as direct quantum tunneling is present for  $d_{ox} < 2.5nm$ . Hence the value of the tunneling current (color level) will depend upon the applied bias as well as the thickness and integrity of gate oxide.

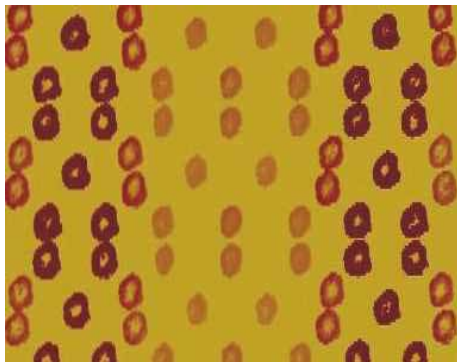


Figure 3: C-AFM current map reveals three types of contact;  $P^+$ ,  $N^+$  and poly contact when applying  $-2V$  to sample stage.

The other unique capability of C-AFM is the ability to obtain local I/V curves of various contacts measured in spectroscopy mode. Figure 4 shows I/V curves obtained with the sample bias ramped from  $-1V$  to  $1V$ . The I/V characteristics of the  $P^+$  contact and  $N^+$  contact look like the behavior of a P/N and a N/P diode respectively. The linear I/V curve of the  $V_{ss}$  contact is the behavior of a resistor. These local I/V curves strengthen further the hypothesis proposed above.

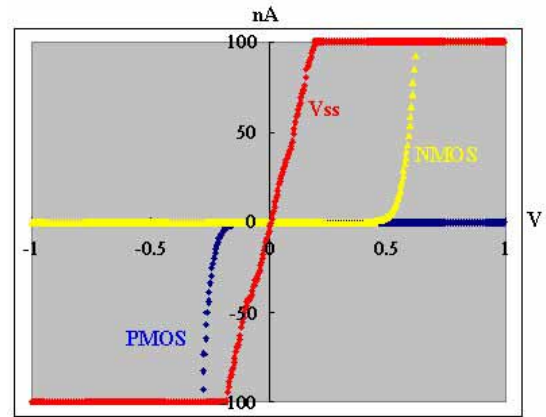


Figure 4: Local I/V spectra show the behavior of diode for contacts of PMOS and NMOS.  $V_{ss}$  contact reveals linear characteristics.

### Gate poly short to $P^+$ contact

A second sample consisting of a  $0.13\mu m$  SRAM with single bit failure was then studied. A memory tester was used to determine the failure address. However no defect was found on the corresponding via and inter-connect metal with the SEM. The sample was parallel lapped to the contact layer and examined by voltage contrast (VC) to identify the faulty contacts. As the voltage contrast image shown in Figure 5 suggests, the poly contact D is brighter than other poly contacts (dark contrast). The VC image implies leakage on that contact. The root cause of the failure might be pinhole induced gate oxide leakage, poly contact short to other contacts or poly residue induced leakage. The VC result alone is not however sufficient to verify the actual failure mechanism and hence, the sample was imaged with C-AFM.

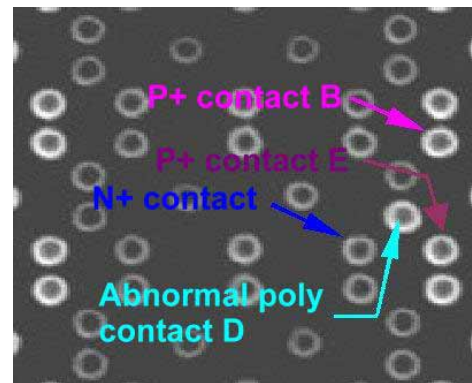


Figure 5: The SEM VC image shows various types of contact. The abnormal poly contact D is easily observed.

Topography and current were measured with an applied bias of  $-2V$ . The current image Figure 6 is consistent with the

previous VC result shown as Figure 5. The failed poly contact D is easily figured out with dark level, and its level is the same as that of P<sup>+</sup> contacts.

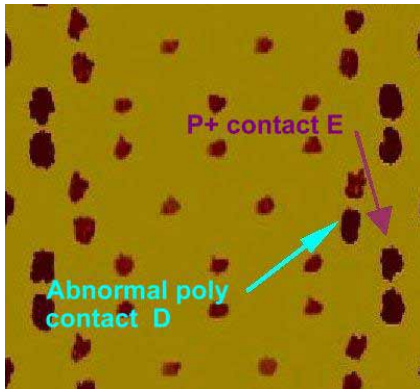


Figure 6: C-AFM current mapping is easy to identify abnormal poly contact D with dark level.

To allow for the diagnosis of the failure mechanism it is important to consider data from multiple contacts I/V data for different contacts were acquired, Figure 7, using spectroscopy mode and sweeping the applied sample bias from -3V to 3V. Curves A, B, C, D and E correspond to N<sup>+</sup> contact, P<sup>+</sup> contact, normal poly contact, abnormal poly contact D and P<sup>+</sup> contact E respectively. Curve D of the failed poly contact is the same as curve B and E of P<sup>+</sup> contact. In addition, the poly contact D is just located close to the P<sup>+</sup> contact E. Based on this data the failure mechanism is most likely the gate poly short to P<sup>+</sup> contact E. After removing ILD with a dilute HF solution SEM data, Figure 8, shows a direct short from the poly to the P<sup>+</sup> contact E due to poly residue. This may be induced by foreign particles during the poly pattern definition.

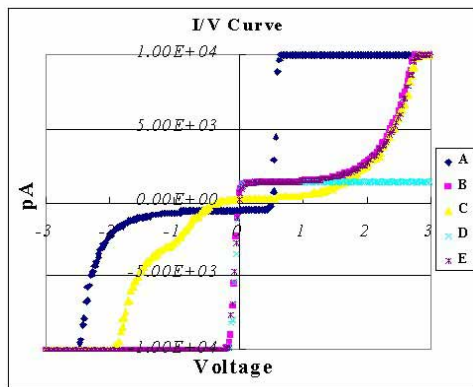


Figure 7: I/V curves measured on different contacts. Curve D and E overlap together, which means these two contacts short together.

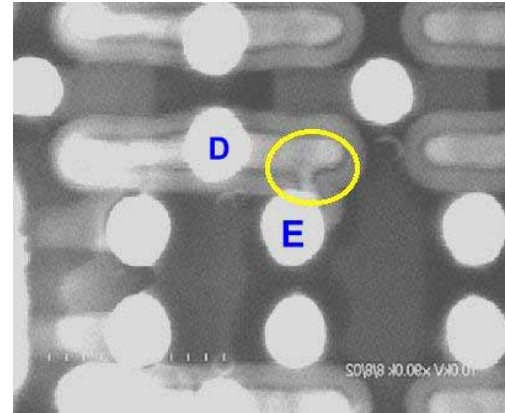


Figure 8: SEM image shows poly and P<sup>+</sup> contact short together due to poly residue.

### CoSi induced junction leakage

This sample is a logic product fabricated using a 0.13um process. The specification for the standby current is 20uA. It was noted that this batch suffered from a higher standby current (~50uA) and hence resulted in a yield loss above 40%.

Dynamic EMMI (Emission Microscope) was first performed on the sample. Emission spots are found on failure samples using test vectors. Hot spots from the same circuit region are not located at the same position for different samples. The suspect circuit is then determined by layout tracing and may be observed by SEM layer by layer. However, no defect was found on the corresponding inter-connect metal, via, contact or poly layers. The sample was subsequently parallel lapped to the contact layer and voltage contrast observation performed. This method did not find any defect. C-AFM data was obtained taken to isolate the defect on the contact level directly.

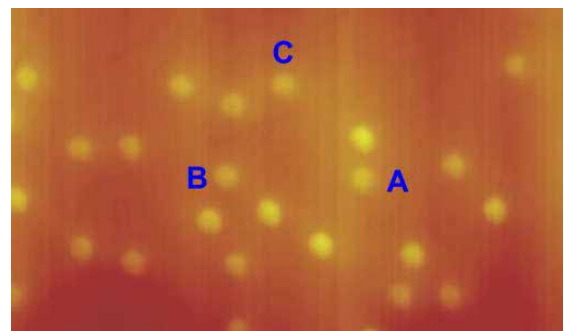


Figure 9: Contact layer topography image captured by C-AFM.

The topography and current map are shown in Figures 9 and 10 respectively. Three abnormal N<sup>+</sup> contacts (A, B, C) were found and are visible in Figure 10 as low contrast regions when the applied sample bias was -1V. This implies micro leakage

exists at the  $N^+$ /P-well junction. Subsequent I/V measurements, Figure 11, show that these  $N^+$  contacts are easy breakdown at sample biases of between  $-0.5V$  and  $-1.5V$ . This is compared to normal  $N^+$  contacts, which are not breakdown even at applied biases of  $-3V$ . Furthermore, TEM data Figure 12 shows the thickness of the CoSi layer of the abnormal contacts is 58nm at the corner of the Active Area (AA), which is deeper than the normal thickness. The deeper CoSi might induce junction leakage and would result in a higher standby current in this case.

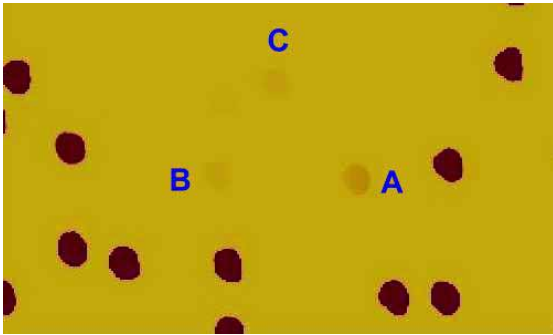


Figure 10: Current mapping shows  $N^+$  contacts A, B, and C show little contrast in the current image. Micro leakage may be the root cause.

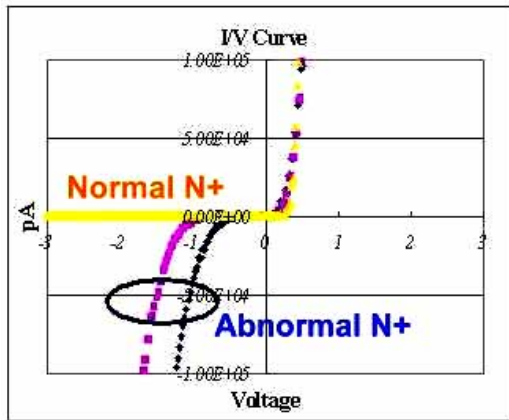


Figure 11: I/V curves show abnormal  $N^+$  contacts are early breakdown at  $-0.5V$  to  $-1.5V$ , but normal  $N^+$  contact is not breakdown even at  $-3V$ .

### Fault localization hit rate

A comparison of the “hit rate” between VC and C-AFM used a total of 33 samples that were parallel lapped to the contact layer. The hit rate of defect identification by using VC and C-AFM are 30% (10/33) and 90% (30/33) respectively, Table 1. The hit rate is sample dependent. On average, C-AFM improved the hit rate of defect isolation above 40% compared to VC.

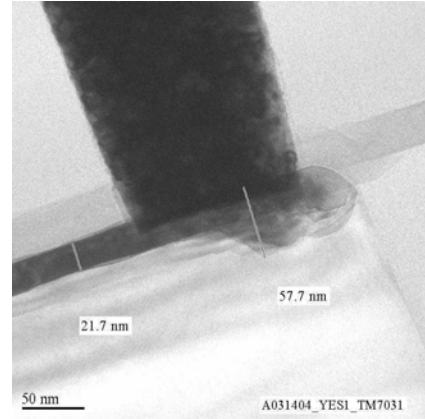


Figure 12: TEM image shows the thicker CoSi thickness on the abnormal contact.

Fail mode	VC Hit rate	C-AFM Hit rate (Qty.)	Result
Iddq fail	0/4	4/4(4)	Some $N^+$ and $P^+$ contacts are leak
Iddq fail	0/6	6/6(6)	Some $N^+$ and $P^+$ contacts are leak
PBL fail	0/1	1/1(1)	BL contact short to WL at Via layer
Scan fail	0/2	2/2(2)	$N^+$ contact is leakage from I/V measurement
FT fail	0/1	0/1(1)	Different I/V curves was found
Function fail	N/A	1/1(1)	Check the behavior of $N^+$ and poly contacts
Function fail	0/1	1/1(1)	Poly contact suffered seriously leaky
Power leakage	5/5	5/5(5)	Some $N^+$ and poly contacts are leak
SB fail	0/1	1/1(1)	The I/V curve reveals the $N^+$ contact is leak
Function fail	0/1	1/1(1)	Poly contact is leak from I/V curve
PBL fail	2/3	2/3(3)	BL contact short to WL at Via layer
Cache fail	0/2	1/2(2)	RC_ poly too high
SB fail	2/2	2/2(2)	Vss contact is short to poly contact
SB fail	0/2	2/2(2)	$N^+$ contact is leak
PBL fail	1/1	1/1(1)	BL short to WL at contact layer.

Table 1: The hit rate comparison table of defect isolation between VC and C-AFM.

### Conclusion

Today’s failure analysis is becoming more and more difficult as devices become smaller. The development of new techniques such as C-AFM will make this job easier.

C-AFM is a popular technique for electrical characterization of dielectric film and gate oxide integrity (GOI). More and more FA laboratories are acquiring this type of tool. In this work, the existing applications of C-AFM were extended to allow defect localization at the contact level with resolutions in nano-meter and pico-amp range. Current mapping easily

identifies faulty contacts with higher contact resistance or micro junction leakage. Local I/V measurement provides information required in order to establish the failure mechanism.

## References

1. Jon C. Lee, C. H. Chen, David Su, J. H. Chuang, "Investigation of Sensitivity improvement on Passive Voltage Contrast for Defect Isolation", ESREF Proceedings (2002)
2. Kenneth Krieg, Richard Qi, Douglas Thomson, Greg Bridges, "Electrical Probing and Surface Imaging of Deep Sub-micron Integrated Circuits", ISTFA Proceedings (1999)
3. Kenneth Krieg, Douglas Thomson, Greg Bridges, "Multiple probe Deep Sub-micron Electrical Measurements Using Leading Edge Micro-machined Scanning Probes", ISTFA Proceedings (2001)
4. Andrew N Erickson, "What Can a Failure Analysis Do with an AFM", ISTFA Proceedings (2002)
5. A.Olbrich, B. Ebersberger, C. Boit, "Local electrical thickness mapping of thin oxides with conducting atomic force microscopy" ISTFA Proceedings (2000)
6. Application Notes, Digital Instruments, Veeco Metrology Group